

Nanoscale

Accepted Manuscript



This is an *Accepted Manuscript*, which has been through the Royal Society of Chemistry peer review process and has been accepted for publication.

Accepted Manuscripts are published online shortly after acceptance, before technical editing, formatting and proof reading. Using this free service, authors can make their results available to the community, in citable form, before we publish the edited article. We will replace this *Accepted Manuscript* with the edited and formatted *Advance Article* as soon as it is available.

You can find more information about *Accepted Manuscripts* in the [Information for Authors](#).

Please note that technical editing may introduce minor changes to the text and/or graphics, which may alter content. The journal's standard [Terms & Conditions](#) and the [Ethical guidelines](#) still apply. In no event shall the Royal Society of Chemistry be held responsible for any errors or omissions in this *Accepted Manuscript* or any consequences arising from the use of any information it contains.



A Self-assembly Aptasensor Based on Thick-shell Quantum Dots for Sensing of Ochratoxin A[†]

Received 00th January 20xx,
Accepted 00th January 20xx

DOI: 10.1039/x0xx00000x

www.rsc.org/chemcomm

Xianfeng Chu,^{a,†} Xiaowen Dou,^{a,†} Ruizheng Liang,^b Menghua Li,^a Weijun Kong,^a Xihui Yang,^a Jiaoyang Luo,^a Meihua Yang^{*a,c} and Ming Zhao^d

A novel self-assembling aptasensor was fabricated by precisely attaching three phosphorothioate-modified capture aptamers onto a single thick-shell quantum dot in a controllable manner for monitoring of Ochratoxin A (OTA), a poisonous contaminate widespread in foodstuffs. Herein, CdSe/CdS QDs coated in ten layer CdS shells were synthesized using a continual precursor injection method. Analysis of the prepared CdSe/CdS QDs showed they contained a zinc-blende structure, high photoluminescence quantum yields (>80%), and a photoemissions peak with a narrow full-width at half-maximum (about 29 nm), all qualities that render them as a superior choice for optical applications. By adjusting the number of phosphorothioate bases in the anchor domain, the tunable-valent aptasensor was able to self-assemble. In the sensing strategy, the thick-shell quantum dot was provided as an acceptor while OTA itself was used as a donor. In the presence of OTA, the capture aptamers drive the aptasensor function into a measurable signal through a fluorescence resonance energy transfer (FRET) system. The newly developed aptasensor had a detection limit as low as 0.5 ng·mL⁻¹, with a linear concentration in the range of 1 to 30 ng·mL⁻¹, and therefore meets the requirements for rapid, effective, and anti-interference sensors for real-world applications. Moreover, the high quality thick-shell QDs provide an ideal alternative for highly sensitive imaging and intensive illumination in the fields of biotechnology and bioengineering.

Introduction

Aptamers have recently drawn considerable interest in the field of biosensor fabrication as emerging sensing elements. Compared to other biological recognition molecules such as antibodies, enzymes, receptors, etc., aptamers provide multiple advantages for use as biosensors, such as relatively easy synthesis, good stability, excellent affinity, and compatibility with diverse modifications.¹ Various aptasensors have already been developed and have been successful in rapidly monitoring contaminants and biomolecules *via* electrochemical,²⁻⁴ colorimetric,^{5, 6} fluorescence,⁷⁻⁹ and other^{10, 11} assays.

Quantum dot (QD)-based aptasensors in particular are regarded as an attractive choice for aptasensor fabrication given the emerging prevalence of QDs in various nanotechnologies.¹²⁻¹⁸ Multiple previously constructed QD-based aptasensors have shown good sensitivity, but have often involved multistep conjugation procedures and necessary purification steps that have led to low

labelling yields. Furthermore, a crucial factor in the quantitative application of this sensing platform is to precisely control the number of aptamers on the QDs.^{19, 20}

Another key issue for aptasensor performance is the optical quality of the QDs. The core-shell QDs possess a high fluorescence quantum yield (QY) and sharp photoemissions,²¹ which have been applied in QD-based aptasensors^{13, 15, 18}. However, few researches focus on the self-properties of the core-shell QDs, such as the thickness of shell layer. Increasing the thickness of shell layer will enhance the specificity of the aptasensor when it was used as one of the key composites for fabricating QLED illumination light source²². This strategy may be a new route in fabricating QD-aptasensors. Generally, thick-shell QDs are prepared using a typical synthetic method of successive ion layer adsorption and reaction (SILAR)²³ under the direction of band gap and composition engineering (BCEN) theory.²⁴ However, some studies have shown that this method leaves large amounts of cadmium precursor in the original CdSe reaction solvent, and leads to the generation of heterostructure nanocrystals, e.g. nanotetrapod structures.²⁵⁻²⁷ Therefore, a core purification step is essential before shell coating in order to synthesize core-shell QDs with high optical quality. However, the necessity of purification is a technical limitations, which results in a time-consuming and labour-intensive synthesis procedure.

Herein, we describe a continual precursor injection method used to synthesize thick-shell CdSe/CdS QDs instead of a

^a Institute of Medicinal Plant Development, Chinese Academy of Medical Sciences & Peking Union Medical College, Beijing 100193, China.

^b State Key Laboratory of Chemical Resource Engineering, Beijing University of Chemical Technology, Beijing 100029, China.

^c Institute of Hainan Branch of Medicinal Plant Development, Chinese Academy of Medical Sciences & Peking Union Medical College, Wanning 571533, China.

^d School of Pharmacy, Jiangsu University, Zhenjiang 212013, China.

[†] X.C. and X.D. contribute equally.

[†] Electronic supplementary information (ESI) available: Tab. S1.

purification process. Increasing the injection amount of Cadmium diethyldithiocarbamate ($\text{Cd}(\text{DDTC})_2$), we succeeded in eliminating the formation of heterostructure nanocrystals, leading to regularly spheroidal CdSe/CdS QDs with a narrow full-width at half-maximum (FWHM) and a high QY. Then, a QD-aptasensor was able to self-assemble due to our design which used different numbers of phosphorothioate bases in an anchor domain. To validate the usefulness of this aptasensor, ochratoxin A (OTA) was selected as a model analyte. OTA is regarded as a potential human carcinogen (group 2B) by the International Agency for Research on Cancer and is often found in foodstuffs²⁸. Tests using the QD-aptasensor with samples of beer demonstrated that the newly developed aptasensor possesses rapid and sensitive response as well as easy operation, giving it great potential for practical applications.

Experimental section

Reagents and materials

Selenium power (Se, 200 mesh, 99.99%) was purchased from Alfa-Aesar. Stearic acid (HSt, 90%), oleylamine (technical grade, 70%), 3-mercaptopropionic acid (MPA, 99%), Rhodamine 6G (R6G, 99%) were obtained from Sigma-Aldrich. Cadmium oxide (CdO , 99.99%) was purchased from Sinopharm Reagents. Cadmium acetate dihydrate ($\text{Cd}(\text{Ac})_2 \cdot 2\text{H}_2\text{O}$, 99%), 1-octadecene (ODE, 90%), Sodium diethyldithiocarbamate trihydrate ($\text{NaDDTC} \cdot 3\text{H}_2\text{O}$, 99%), tetramethylammonium hydroxide (98%) and liquid paraffin were purchased from Aladdin Reagents. All DNA oligonucleotides were synthesized and purified by GENEWIZ Inc. (Suzhou, China). The standards of analogues including Aflatoxins (AFB_1 , AFB_2 , AFG_1 and AFG_2), deoxynivalenol (DON), zearalenone (ZAN), zearalenone (ZON), fumonisin B₁ (FB₁) and fumonisin B₂ (FB₂) and ochratoxin A (OTA) were purchased from Pribolab (Singapore). Caution and safety considerations, necessary precautions should be taken in all operation of the analogues and OTA, which belong to mycotoxins with high toxicity. The commercial beer from supermarket in Beijing (China) was confirmed without the contamination of OTA. Other solvents used were analytical grade and from Sinopharm Reagents. All chemicals were used directly without any further purification unless otherwise stated.

Core/shell CdSe/CdS synthesis

The CdSt_2 and $\text{Cd}(\text{DDTC})_2$ precursors were synthesized according to a method previously reported.²⁹ The CdSe core was prepared using the following procedure. CdSt_2 (1 mmol) and liquid paraffin (20 mL) were loaded separately into a 100 mL three-neck flask. The mixture was placed under a nitrogen flow at 110 °C with continuous stirring for 10 min. The mixture was then heated to 250 °C and the Se precursor solution (prepared previously by dispersing 0.5 mmol of Se powder in 5 mL of liquid paraffin and shaking for 5 min in a vortex) was quickly injected into the reaction flask. The reaction temperature was held at 250 °C to allow for further growth. Needle-tip aliquots were extracted and dissolved in chloroform and used to monitor the progress of the reaction through UV-vis and photoluminescence measurements. When the cores reached the desired size, the reaction mixture was cooled to 50 °C in preparation for the CdS shell coating procedure.

In order to add the CdS shell coating, 25 mL of oleylamine was injected *via* a syringe into the reaction solution (described above), and then heated to 80 °C. A shell precursor solution was made by dissolving 1.23 g of $\text{Cd}(\text{DDTC})_2$ into a mixture of liquid paraffin (21 mL) and oleylamine (7 mL), respectively. This precursor solution was then injected in ten consecutive rounds (0.55, 0.88, 1.5, 2.0, 3.0, 4.0, 5.0, 6.0, 10.0, and 10.0 mL). After the first injection of the $\text{Cd}(\text{DDTC})_2$ solution the temperature of the reaction solution was increased to 160 °C and held there for 25 min. The reaction mixture was then allowed to cool to 80 °C and a second portion of the $\text{Cd}(\text{DDTC})_2$ solution was injected. This injection procedure was repeated nine times, for a total of ten injections, and the CdS shell was allowed to grow at 150 °C for a final 25 min until an approximately ten-monolayer CdS shell had formed. Needle-tip aliquots were taken throughout the procedure in order to monitor the reaction progress using UV-vis and PL measurements. An absorbance value at 450 nm was recorded using an Agilent Cary 100 UV-vis spectrophotometer. The PL spectrum was obtained using a Hitachi F-7000 fluorescence spectrophotometer with an excitation wavelength of 450 nm. The relative QY of the QDs was calculated using the absorbance and PL values by comparison with a standard (R6G). Prior to characterization, each aliquot of solution was dissolved in chloroform, precipitated using acetone, and dried under vacuum. The TEM images were taken on a Hitachi 7700 transmission electron microscope with an acceleration voltage of 100 kV using copper grids (400 mesh) coated with the pure carbon-support film. The XRD patterns were obtained using a Rigaku Ultimate-IV X-ray diffractometer operating at 40 kV/40 mA using Cu K α line ($\lambda = 1.5418 \text{ \AA}$).

Phase transfer of organic CdSe/CdS QDs into aqueous phase

Prior to ligand exchange, the final raw solution was dispersed in an appropriate amount of chloroform and separated using acetone in a centrifuge at 10,000 rpm for 5 min. The precipitate was then re-dispersed in chloroform, and deionized water and MPA were added in sequence. After vortexing, the chloroform layer was discarded and the MPA capped CdSe/CdS QDs were washed three times with ethanol. Finally, water was added to the precipitated QDs, followed by slow addition of NaOH until the solution appeared clear. The MPA-capped QDs were then washed a final time using ethanol and re-dissolved in water.

Self-assembly of a tunable-valency aptasensor based on CdSe/CdS QDs

Initially, the solution of MPA-CdSe/CdS QDs (150 μL) mixed well with 3 mL of buffer solution (10 mM Tris, 30 mM NaCl, pH 8.0). The 1 mL of ssDNA (listed in Table S1) modified with phosphorothioates was then added dropwise into this solution and slowly stirred for 10 h.

Confirmation of the ss-DNA valency on the CdSe/CdS QDs surfaces

In this experiment, the 150 μL of a-ssDNA-CdSe/CdS QDs (aptasensors) and c-ssDNA-CdSe/CdS QDs were added separately into 200 μL of the detection buffer (20 mM PB, 1 mM MgCl_2 , 5 mM KCl, pH 8.0) and incubated for 30 min at room temperature to allow for sufficient hybridization. Formation of the complex was then confirmed using TEM images.

Assay of OTA levels using the developed aptasensor

A series of OTA standard solutions (5 μL , diluted in detection solution in advance) were mixed with 25 μL of aptasensor solution and 470 μL of detection buffer (20 mM PB, 1 mM MgCl_2 , 5 mM KCl, pH 8.0) for 5 min. The PL intensity was then recorded at an emission wavelength of 627 nm using an excitation wavelength of 450 nm.

Preparation of the beer sample

After removing the foam, the beer sample was directly diluted 10 times by buffer solution and filtrated.

Results and discussion

The principle component of the aptasensor design strategy is shown in Fig. 1. In order for the aptasensor to self-assemble, phosphorothioate modified single stranded DNA (Supplementary Tab. S1, a-ssDNA) is used as a binding ligand on the QDs. The a-ssDNA sequence consists of two domains, a sulphur-containing phosphodiester backbone (anchor domain) and an anti-OTA aptamer sequence (functional domain). The anchor domain will preferentially bind to an inorganic surface through the coordination of sulfur to metal ions (e.g. Cd^{2+} ions),¹⁹ and thus provide a strong conjugate. The functional domain is composed of G-rich oligonucleotide sequences which undergo a conformational transition to form G-quadruplexes in the presence of OTA.³⁰ This transformation is due to the high affinity with which the OTA binds the aptamer and pulls the OTA molecule towards the QDs. The OTA and QDs form a donor-acceptor pair in close enough proximity to enable a fluorescence resonance energy transfer (FRET) process. Through monitoring the enhancement of fluorescence of aptasensor based on QDs it is possible to sense the presence of OTA.

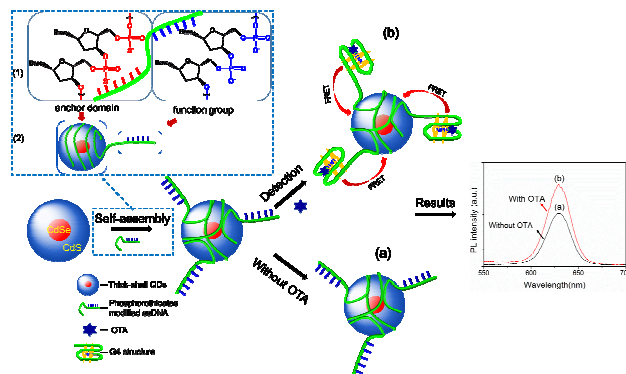


Fig. 1 Schematic illustration of (1 & 2) a self-assembling tunable-valency aptasensor through incubation of QDs with phosphorothioates modified ssDNA and (a & b) the design for monitoring OTA in the system.

The CdSe core QDs were made by injecting a Se suspension into hot cadmium stearate (CdSt_2) solvent and allowed to grow approximately 2 min until the desired size (~ 3.03 nm, Fig. 2) was reached. After this process, residual unreacted selenium as well as CdSt_2 monomer remained in the reaction solution. Unless the unreacted selenium is removed, it will readily induce the formation

of unwanted alloy structure under the high temperature conditions of the subsequent precursor injection step.³¹ To avoid this problem, new precursors for the epitaxial layer of the CdS shell were considered based on their activity at low temperatures.²³ $\text{Cd}(\text{DDTC})_2$ was chosen for use as a shell precursor because it had high enough activity to allow release of one molecule of CdS monomer for CdS coating at reduced temperatures.³¹ In the case of the left over CdSt_2 monomer, an improper dose of the $\text{Cd}(\text{DDTC})_2$ will lead to generation of QD heterostructures because the CdSt_2 possesses a higher chemical potential compared to the shell precursor. As suspected, CdSe/CdS QD nanotetrapods were clearly observed after the 3rd shell precursor injection (Fig. 2) during shell growth. However, transmission electron microscopy (TEM) revealed round QDs instead of tetrapod QDs after the 10th shell-growth injection (Fig. 2), the TEM images of 4th, 6th, and 8th shell precursor injection are provided in support information Fig. S1). This most likely indicates that as the shell thickness increased the potential energy of the ground state on the surface of QDs decreased, thus reducing the “hardness” of the material.³² It is likely that the Gibbs free energy ($\Delta_r G^\circ$) is higher at the surface of the QD nanotetrapods than at the arms, causing the CdS shell to grow more quickly on the surface than on the arms of the QD nanotetrapods.

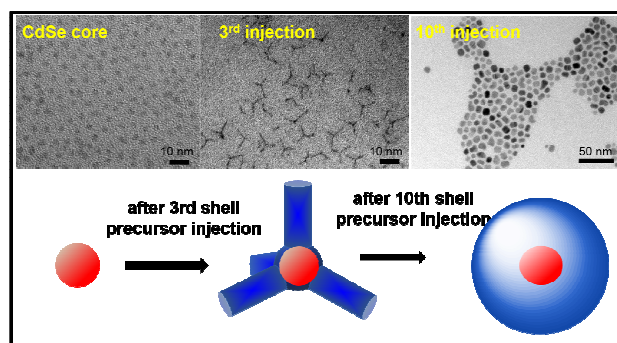


Fig. 2 Top: the TEM images of the CdSe and CdSe/CdS QDs with increased injection times increasing; Bottom: Illustration of the shell growth of CdSe/CdS QDs.

In the reaction system, the use of oleylamine (OAm) as a ligand during the CdS shell-growth stage initiates two antagonistic processes. It accelerates the CdS shell growth by activating the shell precursor, and simultaneously decelerates the shell growth by forming a protective coverage on the QD surfaces. An optimal amount of 35% OAm (v/v) was used during 15 rounds of shell precursor infusion and the formation of nanotetrapods was finally eliminated, as shown in Fig. 3A. However, the quantum yield (QY) had decreased to only 20%. The final QDs with perfect dot morphology (Fig. 3B) and a high QY of more than 80% were obtained by adjusting the amount of $\text{Cd}(\text{DDTC})_2$ after 10 quick rounds of shell-growth. The average particle diameter of the final QDs had extended from 3.03 to 9.8 nm, which is equivalent to a shell thickness of 3.4 nm. According to previous studies^{21, 33}, a monolayer of CdS is approximate to 0.34 nm, therefore, the CdS in our prepared CdSe/CdS QDs can be estimated at 10 layers.

The structure of the core-shell CdSe/CdS QDs was confirmed using X-Ray Diffraction (XRD). As shown in Fig. 3C, the Peak

characteristics indicated that the ensemble of CdSe/CdS QDs have zinc-blende structure, in agreement with a report by Choi et al.³⁴ Moreover, the CdSe/CdS QDs with a quite thick CdS layer, so that there is no typical diffraction peak of corresponded to the zinc-blende CdSe core (green and blue sticks in Fig. 3C and Fig. 3D, respectively). This proved that the CdS growth was performed on core CdSe.³¹ Previous studies of CdSe/CdS nanorods and nanotetrapods have indicated that the shell of CdS preferred to grow into wurtzite phase, both from a wurtzite core CdSe or a zinc-blende core CdSe, by epitaxial growth. Here however the formation of a total zinc-blende structure was in contradiction with other recent results.³⁴ It was noteworthy that the growth temperature for other research was at or above 300 °C for nanotetrapod formation, when fatty amines were used in the present study as activation reagents of the single-source precursor,³⁵ a zinc-blende CdS shell was produced at a lower temperature.

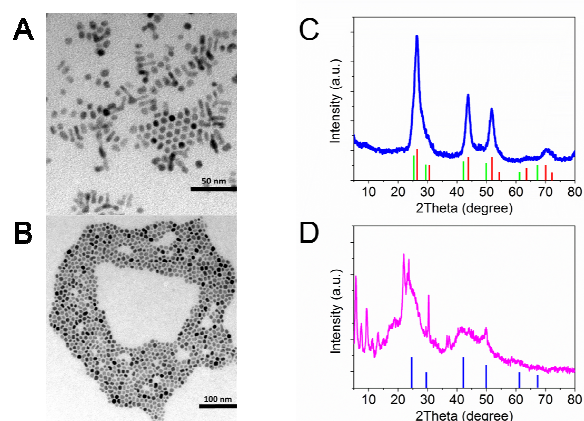
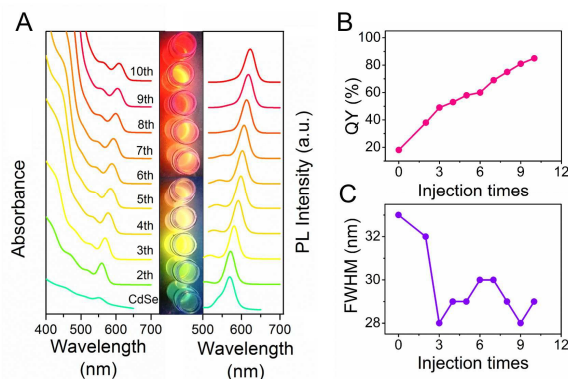


Fig. 3 The TEM images of the final CdSe/CdS QDs with various numbers of injection times (A corresponding to 15 and B to 10 injection times); (C) The XRD patterns of the CdSe/CdS core/shell QDs. Stick patterns show the standard peak positions of bulk zinc-blende CdS (red sticks) and zinc-blende CdSe (green sticks); (D) The XRD patterns of the CdSe core QDs. Stick patterns show the standard peak positions of zinc-blende CdSe (blue sticks)

The optical properties of the prepared QDs were further examined using photoluminescence (PL), absorbance spectra, QY, and measuring the FWHM of PL peaks, as shown in Fig. 4. As the CdS shell grew, a continuous red-shift (Fig. 4A) in the PL and absorbance spectra was observed. This effect resulted from partial leakage of the core CdSe excitons into the CdS shell.³⁶ The QY increased to 80% for the final CdSe/CdS QDs, up from 20% for the core CdSe (Fig. 4B). During shell growth around the core, the FWHM of the PL peaks decreased remarkably, with the minimum FWHM as narrow as 29 nm (Fig. 4C). In addition, this synthesis method eliminated the usually necessary core purification step, the synthesized CdSe/CdS QDs have both narrow PL FWHM and high QY, making them ideal labelling material for aptasensor applications.

Due to OAm coverage on the surface of initially prepared QDs, phase-transfer was necessary for subsequent conjugation and detection in aqueous solution. Coordination between thiols and metal ions has been regarded as an excellent conjugation approach.

As predicted, the addition of 3-mercaptopropionic acid (MPA) successfully pulled the QDs into aqueous phase through the replacement of OAm by MPA, which could be monitored under an ultraviolet lamp (Fig. 5A). Then, the aqueous phase MPA-QDs were able to readily self-assemble into a functionalized aptasensor after incubation with ssDNA that had been modified with



phosphorothioates.

Fig. 4 (A) The UV-visible absorbance and PL spectra of the CdSe and CdSe/CdS QDs recorded for increasing numbers of precursor injection times. The luminescence picture was taken using a 365 nm UV excitation; (B) The quantum yield and (C) the full width at half maximum of the PL spectra for the CdSe and CdSe/CdS QDs as the number of precursor injections increased.

Further binding and capping the ssDNA that contains the functional domain for the QDs would further improve detection sensitivity. However, taking the steric conformation of a biomolecule into consideration,³⁰ an increase in the amount of ssDNA on the surface would probably adversely affect any improvement to sensitivity. These effects could potentially be harmful to the current strategy of constructing aptamer-QDs. To build the tunable-valency ssDNA per QD in a controlled manner, three types of phosphorothioate modified ssDNA were designed on the basis of an anti-OTA aptamer, see Tab S1. Different numbers of phosphorothioate bases on ssDNA (a-ssDNA1, 2, 3) were used to determine the number of ssDNA per QD. The c-ssDNA, which consisted of short complementary oligonucleotide sequences corresponding to a-ssDNA, was used to confirm the valency of ssDNA on the QDs. QDs were first incubated with a-ssDNA, sequentially, c-ssDNA was added and allowed to hybridize. TEM images (Fig. 5B) of the results showed that each QD could bind with one molecule of a-ssDNA1, two molecules of a-ssDNA2, or three molecules of a-ssDNA3. The TEM images with a lower magnification about more QDs complexes were provided in SI (Fig.S2-S4). Tuning the number of phosphorothioate bases on the anchor domain of ssDNA allowed precise binding to the QD surfaces.

To examine the interaction between QDs, PL spectra of QD-QD complexes as well as aptamer-QDs conjugates were compared with spectra of the original QDs. As shown in Fig. 5C (taking a-ssDNA3-QDs for an example), there is little change of the PL spectra from either the formation of QD-QD complexes or the aptamer-QDs conjugates. These results demonstrate that no interaction between multiple QDs in the extremely short distance and that the modified

ssDNA had no influence on the PL spectra of the QDs. The CdS shell thickness of the as-prepared CdSe/CdS QDs is estimated to be about 3.4 nm, making adjacent cores about 6.8 nm apart. The effective distance between donor and acceptor for FRET to take place is theoretically less than 6.8 nm. The strategy presented here uses a simple operation rendering and is promising for FRET mechanisms used in nanotechnology.

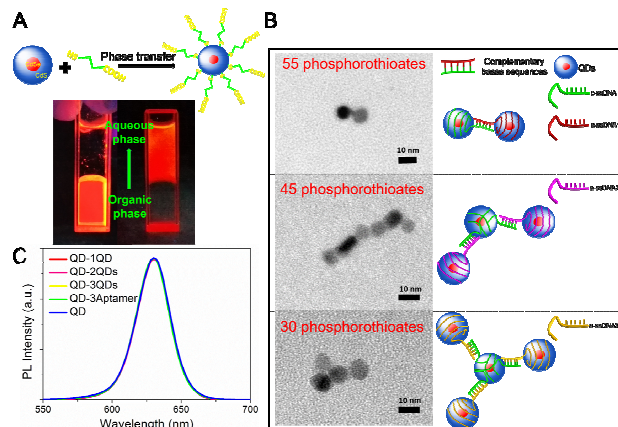


Fig. 5 (A) Top: An illustration of phase transfer using MPA; Bottom: before (left) and after (right) phase transfer; (B) TEM images of QD-QD complexes and their schematic representations; (C) PL spectra of QD-QD complexes, aptamer-QD conjugates, and the aqueous QDs solution.

Coagulation of QDs based conjugates will influence the sensing results, particularly under harsh conditions. In order to test the stability of the prepared aptamer-QDs (aptasensors), buffer solution containing NaCl (1M) was added into an aqueous solution of aptamer-QDs and MPA-capping QDs. Remarkably, the initial QDs immediately coagulated at the bottom of the tube while the aptasensors remained well dispersed in solution. These results were consistent with images taken under an ultraviolet lamp (Fig. 6A), and demonstrated that the prepared aptasensor is resistant to high-salt environment.

To illustrate the sensing concept of the aptasensor, the UV-vis spectrum of the aptasensor and the PL spectrum of OTA were collected. As seen in Fig. 6B, the fluorescence emission spectrum of OTA has a broad overlap with the absorption spectrum of the aptasensors based on CdSe/CdS QDs. Provided the functional domain of the aptasensor binds OTA, it is possible that FRET occurs from the OTA to the QDs of the aptasensor. Results shown in Fig. 6C confirm this hypothesis, as the fluorescence intensity of the aptasensor based on a-ssDNA3 dramatically increased in the presence of OTA as compared to that of the aptasensor alone. Another effect may also contribute to the enhancement of the FRET effect. Upon OTA binding the 5'-end of the anti-OTA aptamer folds into a rigid antiparallel G-quadruplex structure.^{27, 34} Furthermore, the fluorescence intensity of OTA could be enhanced by the G-G base pairs through π -stacking,³⁷ or overall motion restriction.³⁵

It has been noted that FRET should take place from OTA directly to the surface of the QDs. sA-ssDNA, which contains 55 phosphorothioate adenosine bases instead of a function group, links with QDs to form a sA-ssDNA-QDs complex. The spectra of the sA-ssDNA-QDs complex showed no difference between before and

after the addition of OTA (100 ng·ml⁻¹), as shown in Fig. 6D. Increasing the concentration of OTA, it had a negligible influence on the PL spectra of the sA-ssDNA-QDs complex (Fig. 6E and 6F). The following interpretation may be responsible for the results: (i) the high affinity of aptamer on the surface of QDs towards OTA, (ii) OTA remains a suitable distance with QDs to produce the effective FRET. The distance-based FRET efficiency is likely reduced by a long distance between the OTA donor and QD acceptors. When an aptasensor functionalized with a-ssDNA (1, 2, or 3) is able to satisfy the effective FRET distance upon OTA binding, and is improved by the formation of G-quadruplexes. The results of these tests validate the usefulness of this aptasensor for monitoring OTA.

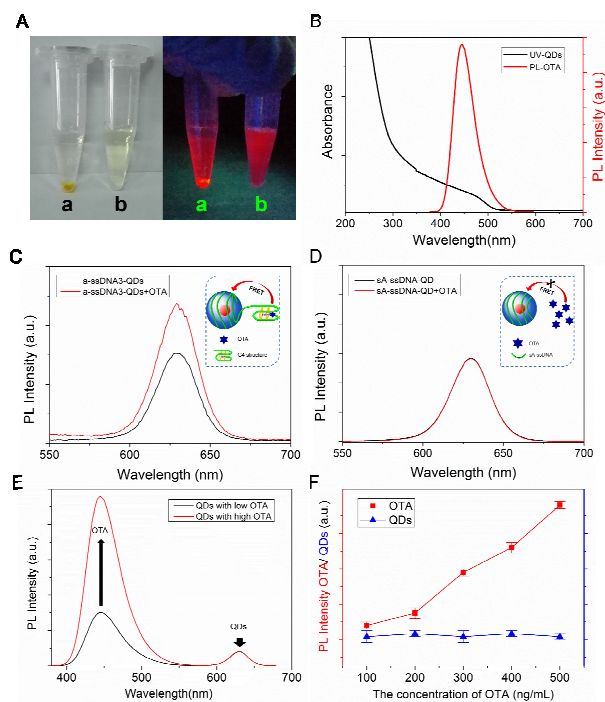


Fig. 6 (A) MPA-QDs (a) and QD based aptasensors (b) in 1M NaCl, photographs taken in bright field (left) and under an ultraviolet lamp (right); (B) The UV-vis absorption spectrum of the QDs (blue line) and the PL spectrum of OTA (red line); (C) PL spectra of the aptasensor based on a-ssDNA3 before (black line) and after (red line) the addition of OTA as well as a schematic illustration of how the aptasensor senses OTA (inset); (D) PL spectra of a sA-ssDNA based aptasensor before (black line) and after (red line) the addition of OTA; (E) PL spectra of the sA-ssDNA-QD complex after additions of OTA of 100 ng/mL (black line) and 500 ng/mL (red line); (F) the PL intensity of the sA-ssDNA-QDs complex (blue line) after addition of various concentrations of OTA (red line).

The monovalent a-ssDNA1 labelled QD aptasensors displayed poor fluorescence enhancement (~10%) in comparison with the trivalent aptasensor (35%) at the same concentration of OTA. Due to the greater sensitivity, the trivalent aptasensor based on a-ssDNA3 was further investigated. In order to better understand the response of the aptasensor to different levels of OTA, concentrations of OTA ranging from 1 ng·ml⁻¹ to 30 ng·ml⁻¹ were carefully added to the aptasensor. The enhancement in fluorescence intensity ($\Delta F = F_t - F_0$) was measured as indicative of aptasensor sensitivity, with F_t and F_0 referring to the fluorescence

intensity of the aptasensor at 627 nm after and before OTA was added, respectively. Results showed that the fluorescence intensity enhancement of the aptasensor had a good linear relationship with the level of added OTA ($\Delta F = 4.75c + 323.18$), with a correlation coefficient (R^2) of 0.9513 in the range of 1–30 $\text{ng}\cdot\text{mL}^{-1}$, Fig. 7A and 7B, with a short period of detection time (~ 2 min). Taking 1% ΔF as the criterion for determining the detection limit, the prepared aptasensor is sensitive to the concentration as low as 0.5 $\text{ng}\cdot\text{mL}^{-1}$ of OTA. To validate the anti-interference capability, analogues of OTA and beer samples were mixed with the aptasensor, respectively. Those interfering substances also mixed together with OTA, and incubated with the aptasensor. Further investigations tested by analogues of OTA as well as a commercial beer sample demonstrated the high selectivity and anti-interference of the aptasensor (Fig. 8). Compared with previous aptasensors for OTA, the sensing system provides a simple, convenient way, and achieves an excellent sensitivity.^{38,39}

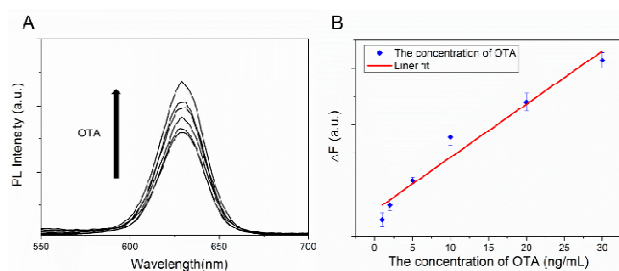


Fig. 7 (A) The PL intensity of the QD based aptasensor mixed with various concentrations (1, 2, 5, 10, 20 and 30 $\text{ng}\cdot\text{mL}^{-1}$) of OTA; (B) the calibration curve of OTA concentration determined using the aptasensor. Error bars represent standard deviations ($n = 6$).

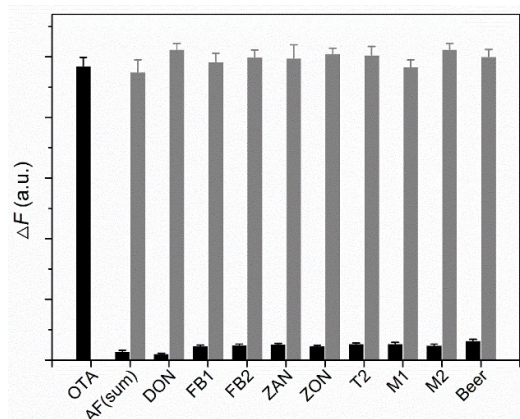


Fig. 8 The fluorescence enhancement of the aptasensor by separately adding of OTA, the analogues, the blank beer (blank) and the mixture of OTA with the analogues or the blank beer (gray). Error bars refer to standard deviations ($n = 3$).

Conclusion

A novel fluorescence assay strategy was developed to sense OTA using a self-assembled aptasensor. CdSe/CdS QDs with CdS shells (approx. ten layers) were synthesized which overcomes the necessity of core purification limitations but still possessing high

quality properties. This synthesis process is probably suitable for large-scale (tens to hundreds of kilograms) industrial preparation of high-quality QDs. Precise control of the aptamers labelled per CdSe/CdS QD was achieved by regulating the number of phosphorothioate oligonucleotides on the anchor domain. This fabrication concept may also be a powerful tool for other FRET mechanism studies using nanotechnology. In this work, a trivalent aptasensor was able to successfully self-assemble and demonstrated promise as a sensing method for real-world applications.

Acknowledgements

This work was supported by National Natural Science Foundation of China (81274072, 81573595, 81473346), Beijing Natural Science Foundation (7152101), Specialized Research Fund for Major Science and Technology Program of Hainan, China (ZDX2013008).

References

- 1 S. D. Jayasena, *Clin. Chem.*, 1999, **45**, 1628.
- 2 L. Huang, J. Wu, L. Zheng, H. Qian, F. Xue, Y. Wu, D. Pan, S. B. Adeloju and W. Chen, *Anal. Chem.*, 2013, **85**, 10842.
- 3 O. S. Kwon, S. J. Park, J. Y. Hong, A. R. Han, J. S. Lee, J. S. Lee, J. H. Oh and J. Jang, *ACS Nano*, 2012, **6**, 1486.
- 4 Y. L. Zhang, Y. Huang, J. H. Jiang, G. L. Shen and R. Q. Yu, *J. Am. Chem. Soc.*, 2007, **129**, 15448.
- 5 Z. Mei, H. Chu, W. Chen, F. Xue, J. Liu, H. Xu, R. Zhang and L. Zheng, *Biosens. Bioelectron.*, 2013, **39**, 26.
- 6 X. Zhang, K. Xiao, L. Cheng, H. Chen, B. Liu, S. Zhang and J. Kong, *Anal. Chem.*, 2014, **86**, 5567.
- 7 X. Liu, R. Freeman, E. Golub and I. Willner, *ACS Nano*, 2011, **5**, 7648.
- 8 H. Cho, E. C. Yeh, R. Sinha, T. A. Laurence, J. P. Bearinger and L. P. Lee, *ACS Nano*, 2012, **6**, 7607.
- 9 S. H. Cao, W. P. Cai, Q. Liu, K. X. Xie, Y. H. Weng, S. X. Huo, Z. Q. Tian and Y. Q. Li, *J. Am. Chem. Soc.*, 2014, **136**, 6802.
- 10 D. Wu, X. Xin, X. Pang, M. Pietraszkiewicz, R. Hozyst, X. Sun and Q. Wei, *ACS Appl Mater Interfaces*, 2015, **7**, 12663.
- 11 H. Cho, B. R. Baker, S. Wachsmann-Hogiu, C. V. Pagba, T. A. Laurence, S. M. Lane, L. P. Lee and J. B. Tok, *Nano Lett.*, 2008, **8**, 4386.
- 12 V. Bagalkot, L. Zhang, E. Levy-Nissenbaum, S. Jon, P. W. Kantoff, R. Langer and O. C. Farokhzad, *Nano Lett.*, 2007, **7**, 3065.
- 13 A. K. Cheng, H. Su, Y. A. Wang and H. Z. Yu, *Anal. Chem.*, 2009, **81**, 6130.
- 14 M. Wu, E. Petryayeva and W. R. Algar, *Anal. Chem.*, 2014, **86**, 11181.
- 15 A. Numnuam, K. Y. Chumbimuni-Torres, Y. Xiang, R. Bash, P. Thavarungkul, P. Kanatharana, E. Pretsch, J. Wang and E. Bakker, *Anal. Chem.*, 2008, **80**, 707.
- 16 G. Jie, L. Wang, J. Yuan and S. Zhang, *Anal. Chem.*, 2011, **83**, 3873.
- 17 T. Lee, A. K. Yagati, F. Pi, A. Sharma, J. W. Choi and P. Guo, *ACS nano*, 2015, **9**, 6675.
- 18 C.-y. Zhang and L. W. Johnson, *Anal. Chem.*, 2009, **81**, 3051.
- 19 N. Ma, E. H. Sargent and S. O. Kelley, *Nature nanotechnology*, 2009, **4**, 121.
- 20 G. Tikhomirov, S. Hoogland, P. Lee, A. Fischer, E. H. Sargent and S. O. Kelley, *Nature nanotechnology*, 2011, **6**, 485.
- 21 O. Chen, J. Zhao, V. P. Chauhan, J. Cui, C. Wong, D. K. Harris, H. Wei, H. S. Han, D. Fukumura, R. K. Jain and M. G. Bawendi, *Nat Mater*, 2013, **12**, 445.
- 22 X. Dai, Z. Zhang, Y. Jin, Y. Niu, H. Cao, X. Liang, L. Chen, J. Wang and X. Peng, *Nature*, 2014, **515**, 96.
- 23 J. J. Li, Y. A. Wang, W. Guo, J. C. Keay, T. D. Mishima, M. B. Johnson and X. Peng, *J. Am. Chem. Soc.*, 2003, **125**, 12567.
- 24 X. Peng, *Acc. Chem. Res.*, 2010, **43**, 1387.
- 25 W. Y. Wu, M. Li, J. Lian, X. Wu, E. K. Yeow, M. H. Jhon and Y. Chan, *ACS nano*, 2014, **8**, 9349.
- 26 D. C. Lee, I. Robel, J. M. Pietryga and V. I. Klimov, *J. Am. Chem. Soc.*, 2010, **132**, 9960.

- 27 A. Fiore, R. Mastria, M. G. Lupo, G. Lanzani, C. Giannini, E. Carlino, G. Morello, M. De Giorgi, Y. Li and R. Cingolani, *J. Am. Chem. Soc.*, 2009, **131**, 2274.
- 28 P. Krogh, *Food Chem. Toxicol.*, 1992, **30**, 213.
- 29 C. Pu, J. Zhou, R. Lai, Y. Niu, W. Nan and X. Peng, *Nano Research*, 2013, **6**, 652.
- 30 B. Prieto-Simón and J. Samitier, *Anal. Chem.*, 2014, **86**, 1437.
- 31 W. Nan, Y. Niu, H. Qin, F. Cui, Y. Yang, R. Lai, W. Lin and X. Peng, *J. Am. Chem. Soc.*, 2012, **134**, 19685.
- 32 J. Aldana, N. Lavelle, Y. Wang and X. Peng, *J. Am. Chem. Soc.*, 2005, **127**, 2496.
- 33 J. van Embden, J. Jasieniak and P. Mulvaney, *J. Am. Chem. Soc.*, 2009, **131**, 14299.
- 34 C. L. Choi, K. J. Koski, S. Sivasankar and A. P. Alivisatos, *Nano Lett.*, 2009, **9**, 3544.
- 35 D. Chen, F. Zhao, H. Qi, M. Rutherford and X. Peng, *Chem. Mater.*, 2010, **22**, 1437.
- 36 S. Deka, A. Quarta, M. G. Lupo, A. Falqui, S. Boninelli, C. Giannini, G. Morello, M. De Giorgi, G. Lanzani and C. Spinella, *J. Am. Chem. Soc.*, 2009, **131**, 2948.
- 37 J. C. Genereux and J. K. Barton, *Chem. Rev.*, 2009, **110**, 1642.
- 38 C. Yang, V. Lates, B. Prieto-Simon, J. L. Marty and X. Yang, *Biosens. Bioelectron.*, 2012, **32**, 208.
- 39 J. Zhang, X. Zhang, G. Yang, J. Chen and S. Wang, *Biosens. Bioelectron.*, 2013, **41**, 704.